

# Tokamak-like confinement at high beta and low field in the reversed field pinch

J S Sarff<sup>1</sup>, J K Anderson<sup>1</sup>, T M Biewer<sup>1</sup>, D L Brower<sup>2</sup>, B E Chapman<sup>1</sup>,  
P K Chattopadhyay<sup>1</sup>, D Craig<sup>1</sup>, B Deng<sup>2</sup>, D J Den Hartog<sup>1</sup>, W X Ding<sup>2</sup>,  
G Fiksel<sup>1</sup>, C B Forest<sup>1</sup>, J A Goetz<sup>1</sup>, R O'Connell<sup>1</sup>, S C Prager<sup>1</sup> and  
M A Thomas<sup>1</sup>

<sup>1</sup> Department of Physics, University of Wisconsin, 1150 University Avenue, Madison, WI 53706, USA

<sup>2</sup> Electrical Engineering Department, University of California, Los Angeles, CA, USA

E-mail: jssarff@wisc.edu

Received 11 July 2003

Published 13 November 2003

Online at [stacks.iop.org/PFCF/45/A457](http://stacks.iop.org/PFCF/45/A457)

## Abstract

For several reasons, improved-confinement achieved in the reversed field pinch (RFP) during the last few years can be characterized as 'tokamak-like'. Historically, RFP plasmas have had relatively poor confinement due to tearing instability which causes magnetic stochasticity and enhanced transport. Tearing reduction is achieved through modification of the inductive current drive, which dramatically improves confinement. The electron temperature increases to  $>1$  keV and the electron heat diffusivity decreases to  $\sim 5 \text{ m}^2 \text{ s}^{-1}$ , comparable with the transport level expected in a tokamak plasma of the same size and current. This corresponds to a 10-fold increase in global energy confinement. Runaway electrons are confined, and Fokker–Planck modelling of the electron distribution reveals that the diffusion at high energy is independent of the parallel velocity, uncharacteristic of stochastic transport. Improved-confinement occurs simultaneously with increased beta  $\sim 15\%$ , while maintaining a magnetic field strength ten times weaker than a comparable tokamak. Measurements of the current, magnetic, and electric field profiles show that a simple Ohm's Law applies to this RFP sustained without dynamo relaxation.

## 1. Introduction

A toroidal plasma configuration in which the strength of the magnetic field is minimized, both to increase beta (plasma pressure normalized to magnetic pressure) and to decrease the engineering demands on the magnets, could minimize the cost of a fusion power core. Typically, however, the confinement of fusion-relevant plasmas is more challenging when the magnetic field is reduced. For example, the reversed field pinch (RFP) configuration, one of the better-studied lower field configurations, historically has had relatively poor confinement as a

result of instabilities that cause the magnetic field to become stochastic. In contrast, tokamak and stellarator configurations more readily achieve fusion-relevant confinement in part through application of a strong magnetic field generated external to the plasma, making them more robust to deleterious modification by magnetic instabilities in the plasma. The optimization of externally magnetized plasmas therefore tends to maximize the available field strength, which is primarily an engineering and cost issue.

In the last few years, a dramatic improvement in the confinement of RFP plasmas has been demonstrated by reducing the magnetic instabilities tending to appear in weakly magnetized plasmas [1–5]. For several reasons, this improved-confinement can be described as ‘tokamak-like’ in comparison with externally magnetized plasmas. In Madison Symmetric Torus (MST) plasmas [4], for example, the electron temperature profile is peaked (instead of flat as in standard RFP plasmas). Also, the electron heat diffusivity falls to  $\chi_e \sim 5 \text{ m}^2 \text{ s}^{-1}$ , which is comparable with the transport level measured in the same size and current tokamak plasmas. The global confinement increases 10-fold, likewise becoming comparable with tokamak scaling expectations for the same size and current plasma. Fast electrons are confined [6], indicative of reduced magnetic stochasticity and restoration of at least some closed magnetic surfaces, as exist in strongly magnetized plasmas. The total beta value is increased to  $\beta_{\text{total}} \sim 15\%$  with Ohmic heating alone, which is as large (or larger) than the  $\beta_{\text{total}}$  demonstrated in advanced tokamak plasmas with powerful auxiliary heating. A beta limit for the RFP has not been identified experimentally, and that achieved is thought to be its natural value for Ohmic heating. A relatively smaller magnetic field strength has been maintained in the RFP while achieving this improved-confinement and beta; a comparable tokamak would have a ten times larger magnetic field at the surface for typical operation with edge safety factor  $q_a = 4$ .

This paper describes results for improved-confinement RFP plasmas obtained in the MST. A main theme is contrasting the key differences between improved-confinement and standard RFP plasmas. New measurements of the inductive electric field profiles and analysis of Ohm’s Law for the parallel current are highlighted, as are measurements that demonstrate a correlation of high core temperature and small amplitude modes resonant in the middle region of the plasma. For completeness, other published results are reviewed that collectively support a characterization of RFP confinement as approaching tokamak-like.

## 2. Inductive current drive and Ohm’s Law

The MST [7] produces circular cross-section toroidal plasmas with dimensions  $R = 1.5 \text{ m}$  and  $a = 0.5 \text{ m}$  (large for RFP experiments) and with toroidal plasma current  $I_\phi \leq 0.5 \text{ MA}$ . Deuterium plasmas are typically formed. Below we describe the formation of standard RFP plasmas in MST, i.e. those generated by steady toroidal induction, and the formation of improved-confinement RFP plasmas in which the inductive current drive is modified to create plasmas with reduced tearing instability.

### 2.1. Standard RFP formation

Standard RFP plasmas are created by simple toroidal induction, which produces in MST a current pulse lasting  $\approx 60 \text{ ms}$ , with a constant current flattop of  $\approx 30 \text{ ms}$ . Since the RFP’s toroidal magnetic field decreases with minor radius and reverses sign in the edge, the parallel inductive electric field,  $E_{\parallel} = \mathbf{E} \cdot \mathbf{B}/B$ , during the current flattop is peaked at the magnetic axis, decreases with radius, and becomes negative in the edge. This tends to overdrive current in the core and underdrive current in the outer region of the plasma, leading to MHD tearing instability from the gradient,  $\nabla_r(\mathbf{J} \cdot \mathbf{B}/B^2)$  [8].

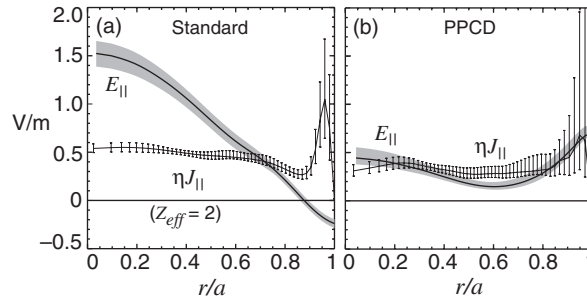


**Figure 1.** Ohm's Law for the parallel current in (a) standard RFP plasmas and (b) PPCD plasmas in MST. The standard plasma data are taken during the current flattop between large bursts of dynamo activity. The PPCD plasma data are taken at 15 ms, midway through the PPCD phase.

A hallmark feature of standard RFP plasmas is the inequality  $E_{\parallel} \neq \eta J_{\parallel}$  in Ohm's Law for the parallel current. Analysis of Ohm's Law for 0.4 MA MST plasmas [9] with line-averaged density  $n = 1 \times 10^{19} \text{ m}^{-3}$  is shown in figure 1(a). The magnetic field, electric field, and current density profiles are measured by toroidal equilibrium reconstructions [10] constrained with a variety of diagnostics. In particular, 11 chords of Faraday rotation measurements from an FIR laser polarimeter [11] together with a single-point motional Stark effect measurement of the magnetic field on axis [12] (using a hydrogen diagnostic neutral beam) provide the primary magnetic profile information. The electron temperature profile is measured using single-point Thomson scattering moved to different radii shot-by-shot, and so the results in figure 1 represent a shot average. The effective charge,  $Z_{\text{eff}}$ , has not been measured accurately in standard MST plasmas, but power balance implies  $Z_{\text{eff}} \sim 2$ , which is the (constant) value assumed in evaluating  $\eta$ . The neo-classical correction for trapped electrons is included, which increases the resistivity by up to a factor of 2, depending on the local trapped electron fraction. The density profile is measured with 11 chords of FIR interferometry [3].

At only one radial location in the standard RFP plasma does  $E_{\parallel} = \eta J_{\parallel}$ . The difference elsewhere is balanced by a magnetic dynamo associated with tearing instability. The required presence of a dynamo is especially clear in the outer region of the plasma where the parallel induction is weak. Note that no realistic  $Z_{\text{eff}}$  is capable of producing  $E_{\parallel} = \eta J_{\parallel}$  near and outside the toroidal reversal surface where  $E_{\parallel} < 0$ . In the simplest three-dimensional resistive MHD model for the dynamo, the surface-averaged fluctuation-induced emf,  $\langle \tilde{\mathbf{V}} \times \tilde{\mathbf{B}} \rangle_{\parallel}$ , balances Ohm's Law, where  $\tilde{\mathbf{V}}$  and  $\tilde{\mathbf{B}}$  are the flow velocity and magnetic field fluctuations associated with resistive tearing modes [8]. Direct measurements of  $\langle \tilde{\mathbf{V}} \times \tilde{\mathbf{B}} \rangle_{\parallel}$  at a few radial locations confirm its existence [13, 14], but this complicated nonlinear physics remains an active area of research both experimentally and theoretically.

Although the self-generated dynamo is a complicated process, it simplifies RFP formation by driving current where toroidal induction is ineffective. Unfortunately a number of tearing modes usually appear, and each mode generates a magnetic island that can easily overlap with a neighbouring mode's island. The resulting magnetic stochasticity enhances energy and particle transport. In fact, the electron heat diffusivity profile determined by power balance in standard MST plasmas agrees very well with stochastic transport expectations [15]. The path forward to fusion-grade plasma confinement for the standard RFP operating with such a multi-helicity dynamo depends on a reduction of the magnetic fluctuation amplitude and stochasticity as the resistivity decreases (Lundquist number increases). However, results to date show a weak Lundquist number scaling for the magnetic fluctuation amplitude [16, 17], implying a large current and/or plasma size to achieve a high temperature.

A different kind of dynamo produced by only one large tearing mode has been observed in MHD computation [18, 19]. This is called the single-helicity dynamo, and it has significant confinement implications for a self-organized RFP. The broadband set of modes that occur for the standard, multi-helicity dynamo have zero (or small) amplitude in the single-helicity dynamo, and so magnetic stochasticity vanishes (or is greatly reduced). The single-helicity dynamo has not yet been observed in RFP experiments, but in some circumstances one mode spontaneously grows larger, while the others remain about the same amplitude. This is thought to be a partial transition to single-helicity [20]. A further description of the single-helicity possibilities for the RFP is included in the section 5.

## 2.2. Pulsed poloidal current drive

The recognition that steady toroidal induction cannot produce a tearing-stable current profile in the RFP suggests modification of the current drive scenario. In particular, figure 1(a) shows that the parallel current drive is too weak in the outer region of the plasma. This can be corrected inductively by imposing a toroidal flux change to generate a poloidal component to the electric field [21], although not in stationary conditions since the toroidal flux embeds the plasma and therefore modifies the magnetic equilibrium. More precise control via RF current drive is theoretically possible since it can be directed to a particular radial location by proper choice of the RF wave properties [22, 23]. An RF drive would also not necessitate a time-varying magnetic equilibrium.

Figures 2 and 3 illustrate a modified inductive current drive developed over the past several years that leads to reduced tearing instability and improved-confinement in MST [1, 4]. This is called pulsed poloidal current drive (PPCD). Figure 2(a) shows an overlay of the toroidal magnetic field applied at the plasma boundary for standard and PPCD conditions at 0.4 MA. To generate PPCD, the toroidal field, i.e. the poloidal current in the toroidal magnet, is ramped negative to create poloidal induction within the plasma. This differs from standard flattop operation, in which the toroidal field is held constant. The PPCD ramp begins at 10 ms and lasts about 8 ms. An important refining ingredient in the PPCD inductive programming that is not shown here is a slow decrease in the applied toroidal loop voltage simultaneous to the poloidal current ramp, eventually going negative,  $E_\phi(a) < 0$ , at  $\sim 16$  ms [4]. This helps to

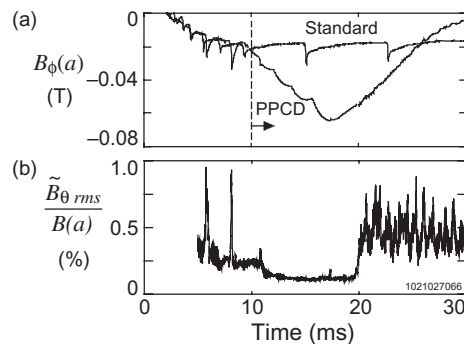


**Figure 2.** (a) Overlay of the applied toroidal field at the plasma surface for standard and PPCD formation. The 'bumpy' PPCD ramp is driven by a five-stage capacitor network in the toroidal magnet circuit. The occasional negative-going spikes in the standard plasma waveform result from the circuit's inductive back-reaction to sudden flux generation events (sawteeth) initiated in the plasma. (b) The spatial rms poloidal magnetic fluctuation amplitude, which indicates the poloidal mode  $m = 1$  magnetic fluctuations.

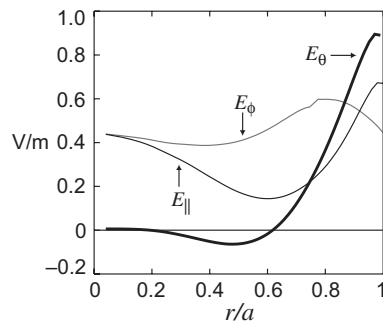


**Figure 3.** Radial profiles of the poloidal ( $E_\theta$ ), toroidal ( $E_\phi$ ), and parallel ( $E_\parallel = \mathbf{E} \cdot \mathbf{B}/B$ ) electric field at 15 ms during PPCD.

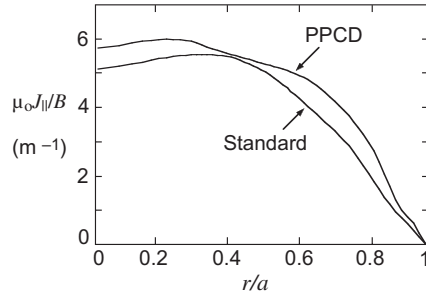
maintain  $E_\parallel(a) > 0$  for a longer period of time to extend the fluctuation suppression period. Figure 2(b) shows the spatial root-mean-square (rms) poloidal magnetic fluctuation amplitude measured with a toroidal array of 32 magnetic sensors located at the plasma surface. (The fluctuation amplitude at the surface is dominated by modes resonant in the core.) Observe that while the poloidal current is ramped, the magnetic fluctuation amplitude is reduced. The data in figure 2 are for a single plasma in which PPCD is especially effective. The degree of fluctuation reduction varies shot-to-shot, especially the time when the fluctuation amplitude decreases to its lowest value, which can be delayed from the start of PPCD by several milliseconds.

Figure 3 shows the inductive electric field profiles at 15 ms during PPCD, obtained from toroidal equilibrium reconstructions incorporating the diagnostic set described above. A novel feature in these reconstructions, however, is that the electric field comes from direct fitting of the time derivative of the Grad–Shafranov equation, not by finite-differencing a time sequence of separate reconstructions [10]. This provides a more accurate determination of the electric field.

The major change in the PPCD inductive current drive scenario is finite  $E_\theta$  to support directly the current in the outer region of the plasma. As a result, the  $E_\parallel(r)$  profile is much flatter than for steady toroidal induction. Analysis of Ohm's Law for the parallel current in PPCD plasmas is shown in figure 1(b), revealing the equality  $E_\parallel = \eta J_\parallel$  to within error bars. Any residual dynamo must be small. For PPCD plasmas the  $Z_{\text{eff}}$  profile determined from near-infrared bremsstrahlung measurements is used to evaluate  $\eta$ . (This technique fails in standard plasmas because a high level of neutral molecular radiation contaminates the bremsstrahlung measurement.) Hence all the components in Ohm's Law are measured for PPCD plasmas [9].

### 2.3. Comparison of $J_\parallel/B$ profiles

The side-by-side comparison of Ohm's Law in figure 1 illustrates that the greatest change in going from standard to PPCD formation is the current drive, not the current profile. The current profile in a standard RFP plasma is, of course, linearly unstable to at least a few tearing modes, but the dynamo provides strong current-flattening feedback, which keeps the profile from ranging far from marginal stability. An overlay of the  $J_\parallel/B = \mathbf{J} \cdot \mathbf{B}/B^2$  profiles for standard and PPCD plasmas is shown in figure 4, obtained from the toroidal equilibrium reconstructions [11]. There is a small increase everywhere in radius, but the profiles are characteristically more similar than dissimilar. Nevertheless, the tearing fluctuations, whose free energy source is  $\nabla_r(J_\parallel/B)$ , are reduced. A 3-fold (or larger) reduction in the magnetic fluctuation amplitude is measured directly in the core by Faraday rotation via fast laser polarimetry [24]. Improved



**Figure 4.** Radial profiles of  $J_{\parallel}/B = \mathbf{J} \cdot \mathbf{B}/B^2$  for standard and PPCD plasmas. The radial gradient,  $\nabla_r(J_{\parallel}/B)$ , is the primary free energy source for resistive MHD tearing at a low beta.

tearing stability is implied. In contrast to the relatively small change in  $J_{\parallel}/B$ , the  $E_{\parallel}$  profiles for standard and PPCD plasmas are substantially different (figure 1); i.e. there is a greater change in the current drive.

### 3. Confinement and beta

The electron temperature increases dramatically when magnetic fluctuations are reduced. The  $T_e(r)$  profiles for 0.4 MA standard and PPCD plasmas are compared in figure 5(a). The standard plasma  $T_e(r)$  is measured during the current flattop, and the PPCD plasma  $T_e(r)$  is measured at 18 ms, towards the end of the PPCD period. The line-averaged density  $n = 1 \times 10^{19} \text{ m}^{-3}$  for both cases. The radial resolution in these profiles is the maximum acquired to date for MST, with each data point representing an average measurement for approximately five similar plasmas. These profiles therefore represent average PPCD performance. Construction of  $T_e(r)$  with less radial resolution but using only the best PPCD plasmas (with longest low-fluctuation periods) shows similar core temperatures but larger  $T_e$  in the outer region of the plasma. A maximum  $T_e(0) = 1.3 \text{ keV}$  has been measured in high-quality 0.5 MA PPCD plasmas [25].

Reduced electron heat loss during PPCD is self-evident in figure 5(a): the temperature increases—which decreases the Ohmic heating power—and the temperature gradient extends well into the core. Local transport analysis confirms this result. The toroidal equilibrium reconstructions provide the local Ohmic heating power density,  $\mathbf{E} \cdot \mathbf{J}$ , which does not require precise knowledge of  $Z_{\text{eff}}$ . The electron heat conductivity profiles,  $\chi_e(r)$ , for standard and PPCD plasmas are compared in 5(b). Losses associated with electron–ion collisions, radiation, and thermal convection are subtracted from the input power to isolate the conducted heat flux  $q_e = -\chi_e n \nabla_r T_e$ . A dramatic decrease in  $\chi_e$  is evident during PPCD, especially in the core. The global energy confinement time increases to  $\tau_E \approx 5 \text{ ms}$ , a 5-fold improvement relative to standard plasmas. Selecting the best PPCD plasmas, the global confinement improvement is estimated to be 10-fold with  $\tau_E \approx 10 \text{ ms}$  and minimum  $\chi_e \sim 5 \text{ m}^2 \text{ s}^{-1}$  [25].

The electron temperature is flat in the core of standard plasmas, where the local  $\chi_e$  is very large as a result of magnetic stochasticity. Modelling of the magnetic field for standard plasmas using the measured equilibrium and tearing mode amplitudes, combined with the radial structure for the dominant tearing modes taken from MHD computation at the same Lundquist number and effective aspect ratio, permits a direct evaluation of the magnetic diffusivity,  $D_m$ . The expected transport  $\chi^{\text{st}} = v_{\parallel \text{th}} D_m$  in a stochastic magnetic field [26] agrees very well with the power-balance measured  $\chi_e$  in figure 5(b) for standard plasmas. This comparison is shown in [15]. The magnetic stochasticity extends out to the  $q = 0$  toroidal field reversal surface,

but outside this radius it is reduced. Hence, a significant  $\nabla_r T_e$  gradient exists only in the edge region up to the reversal surface. The dominant energy loss mechanism in the edge region has not been identified.

Unlike for  $T_e$ , the ion temperature does not change significantly during PPCD. Profiles of the majority and carbon impurity ion temperatures are shown in figure 6 for PPCD plasmas. The majority ion (deuteron) temperature is measured by Rutherford (small-angle) scattering of helium neutrals injected by a diagnostic neutral beam [27]. The  $C^{6+}$  temperature is measured by charge exchange recombination spectroscopy (CHERS) using a second hydrogen diagnostic neutral beam. The ions in standard plasmas are clearly anomalously hot. With  $T_i \sim T_e$ , the collisional heating power  $P_{e-i} \propto (T_e - T_i)$  is insufficient to account for even charge exchange losses  $P_{CX} \lesssim 1$  MW. The responsible heating mechanism has not been identified, but it correlates strongly with dynamo activity [28]. For example, in temporal bursts of large dynamo activity,  $T_i > T_e$ , a clear indication of an anomalous energy transfer to ions. During

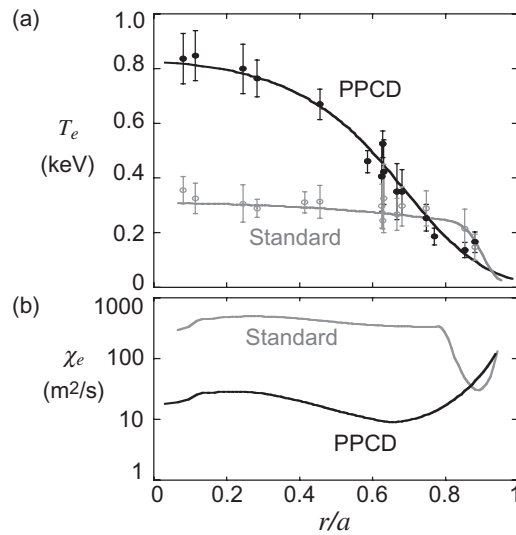


**Figure 5.** (a) Electron temperature profiles for standard and PPCD plasmas at 0.4 MA and density  $n = 1 \times 10^{19} \text{ m}^{-3}$ . (b) Local electron heat conductivity profiles,  $\chi_e$ , for the same conditions.

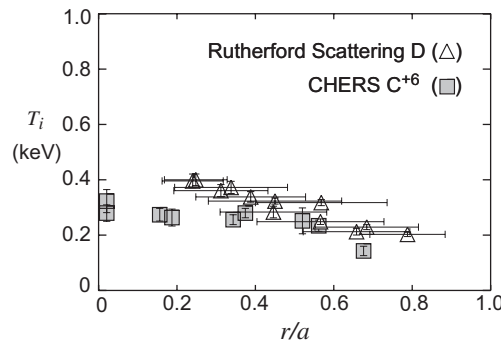


**Figure 6.** Ion temperature profiles for 0.4 MA PPCD plasmas. The majority deuterium temperature is measured by Rutherford scattering, and the minority  $C^{6+}$  temperature is measured by CHERS. These profiles are virtually identical to those measured in 0.4 MA standard plasmas with the density.

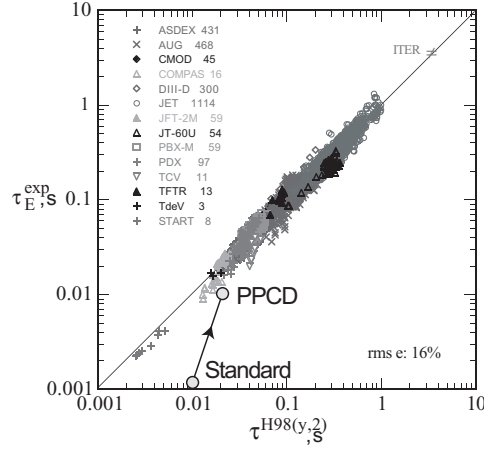


**Figure 7.** MST confinement compared with a ‘fiducial’ tokamak specified by the IPB98(y, 2) ELMMy-H mode empirical scaling (reprinted from ITER Physics Guidelines, ITER report N 19 FDR 1 01-07-13 R 0.1).

PPCD, the larger  $(T_e - T_i)$  difference increases  $P_{e-i}$ , while a drop in neutral density decreases  $P_{CX} \lesssim P_{e-i}$ . The dynamo is also much smaller, perhaps vanishing. Hence, the ions may be only collisionally heated during PPCD, but without better understanding of the anomalous heating mechanism, ion energy transport analysis remains problematic. Note, however, that since stochastic transport is expected to scale with the thermal velocity  $\chi^{st} \propto v_{||th}$ , the expected ion  $\chi_i^{st} = (m_e T_i / m_i T_e)^{1/2} \chi_e^{st}$ . The upper bound for  $\chi_e^{st}$  during PPCD is the power-balance measured  $\chi_e$ , which implies very small  $\chi_i^{st} \lesssim 0.1 \text{ m}^2 \text{ s}^{-1} \sim v_{ie} \rho_i^2$ . The expected stochastic magnetic transport for ions during PPCD is therefore reduced to the classical transport level. The actual  $\chi_i$  is likely to be anomalously larger, of course, perhaps associated with electrostatic turbulent transport as observed in tokamak and stellarator plasmas.

The increase in electron temperature during PPCD leads to a doubling of beta [4]. The maximum beta is achieved in 0.2 MA plasmas, where the total beta,  $\beta_{tot} = \langle p \rangle / B^2(a)$ , increases from 9% in standard plasmas to 15% during PPCD. In higher current 0.4 MA plasmas, the beta enhancement factor is larger, with  $\beta_{tot}$  increasing from 5% to 11%. Hence, the beta reduction observed with increasing current in standard plasmas is lessened with PPCD. For reference, toroidal beta,  $\beta_\phi = \langle p \rangle / B_\phi^2(a)$ , as commonly defined for tokamak and ST experiments, is very large for the RFP since the vacuum (i.e. surface) toroidal field is small ( $\beta_\phi \rightarrow \infty$  by operating with  $q_a \rightarrow 0$ ). During PPCD, toroidal beta decreases to  $\beta_\phi \approx 80\%$  since  $|B_\phi(a)|$  increases. Poloidal beta,  $\beta_\theta = \langle p \rangle / B_\theta^2(a)$ , on the other hand, is much smaller for the RFP since  $B_\theta(a) \approx B(a)$ . There is no clear evidence for a beta limit in either standard or PPCD plasmas. Since beta and confinement are coupled in Ohmically heated plasmas, the observed betas are thought to be their ‘natural’ values. Auxiliary heating is being developed for the RFP only now, which is needed to decouple heating from confinement.

### 3.1. Global confinement comparison with tokamak expectations

The heat conductivity  $\chi_e \sim 5 \text{ m}^2 \text{ s}^{-1}$  observed during PPCD is comparable to that in tokamak plasmas, and therefore the global confinement time is expected to be comparable as well. In principle, the MST could be operated as a tokamak to make a direct comparison in the same device, but tokamak confinement expectations are well documented and quantified in empirical

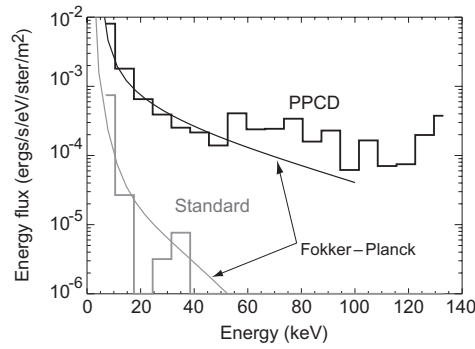


**Figure 8.** Hard-x-ray energy flux spectra for standard and PPCD plasmas. The jagged curves are binned x-ray measurements, and the smooth curves are fits from Fokker-Planck modelling.

scalings representing proper tokamak performance. It is probably better to compare PPCD with a ‘fiducial’ tokamak specified by scaling formulae using MST’s size, current, and other parameters, except for the toroidal field strength, which is chosen appropriate for a tokamak. Such a comparison based on the IPB98(y, 2) ELMy H-mode tokamak empirical scaling is shown in figure 7. The tokamak data come from the ITER physics database used to construct scaling formulae [29]. The data point labelled ‘PPCD’ is  $\tau_E = 10$  ms for  $I_\phi = 0.2$  MA PPCD plasmas plotted against the scaling-projected value  $\tau_E = 23$  ms for the fiducial tokamak derived from the IPB98(y, 2) engineering parameter formula calculated with current 0.2 MA, density  $0.7 \times 10^{19} \text{ m}^{-3}$ , (Ohmic) input power  $P = 0.5$  MW ( $dW_{\text{th}}/dt$  subtracted), major radius, aspect ratio, and circular-shape ( $\kappa = 1$ ). The point labelled ‘Standard’ is MST’s steady-induction confinement  $\tau_E \approx 1$  ms computed in an analogous fashion. The only parameter chosen to be different for the fiducial tokamak is the toroidal field strength  $B_\phi = 1.0$  T, which corresponds to typical tokamak operation with  $q_a = 4$ . The value of the toroidal field is virtually inconsequential, given the IPB98(y, 2) scaling’s weak sensitivity  $\tau_E \propto B_\phi^{0.15}$  (an interesting fact in this comparison). For reference, the L-mode scaling-projected confinement time is  $\tau_E = 18$  ms, and the neo-Alcator (Ohmic) scaling-projected confinement time is  $\tau_E = 31$  ms using similar empirical formulae [29]. These comparisons show that PPCD global RFP confinement is indeed comparable with confinement expectations for a tokamak but with the important difference that  $B(a)$  is ten times smaller in MST as an RFP than it would be as a tokamak of the same size and current. It should be emphasized that the similarity of confinement times does not imply tokamak scaling applies to PPCD RFP plasmas. Too few data exist to draw conclusions regarding the scaling of an RFP with minimized MHD tearing fluctuations, which could be very different from tokamak scalings. It is worth noting, though, that the poloidal gyroradius is the same for tokamak and RFP plasmas if the plasma current, size, and temperature are the same. Banana orbit widths are small in the poloidal-field-dominated RFP, and so the classical transport step-size corresponds to the neo-classical transport step-size in the same size and current tokamak.

### 3.2. Confinement of runaway electrons

Collisionless diffusion in a stochastic magnetic field scales as  $\sim v_{\parallel} D_m$ , where  $v_{\parallel}$  is the parallel particle velocity and  $D_m$  is the magnetic field line diffusivity [26]. The distribution of high-energy electrons is therefore a sensitive indicator of magnetic surface quality. A  $\sim 100$ -fold increase in hard-x-ray bremsstrahlung during PPCD implies that the confinement of high-energy electrons is vastly improved [6]. The x-ray energy flux spectra for standard and PPCD

plasmas are shown in figure 8, measured using a solid state CdZnTe detector [30]. The absence of photons with energy  $\gtrsim 20$  keV in standard plasmas shows that electrons with energy above  $\sim 20$  keV are not confined. In contrast, electrons  $> 100$  keV are present during PPCD. The fast-electron component is  $\sim 20\%$  of the total thermal energy of the plasma, which has not been included in calculations of energy confinement or beta.

Fokker–Planck transport modelling has been used to reconstruct the x-ray flux, thereby inferring the diffusive properties of the collisionless electrons. The multi-species, toroidal, relativistic Fokker–Planck code CQL3D [31] evolves the ion and electron distributions in a Maxwellian background defined by the measured density and temperature profiles. The calculated bremsstrahlung from electron–ion collisions is compared with the measured x-ray flux, and the radial diffusion coefficient is adjusted to match the x-ray emission and, simultaneously, the measured  $E_{\parallel}$  and  $J_{\parallel}$  profiles. The smooth lines overlying the binned experimental data in figure 8 are the best-fit Fokker–Planck reconstructions of the x-ray flux. To achieve reasonable fits, the parallel velocity dependence in the electron diffusion coefficient for standard plasmas is  $D \sim v_{\parallel e}$ , characteristic of transport in a stochastic magnetic field. For the PPCD case,  $D$  is independent of the parallel velocity, implying nonstochastic residual transport. A velocity-independent  $D$  is more characteristic of electrostatic turbulent transport, such as that observed in tokamak and stellarator plasmas.

#### 4. Role of magnetic fluctuation spectrum

The localized nature of resonant field line tearing is well-illustrated in the RFP. Many adjacent modes of significant amplitude are required to diffuse field lines across the radius of the plasma, since  $\mathbf{B}(r)$  is strongly sheared. The RFP's small safety factor  $q(r) < 0.2$  requires  $m = 1$  or 0 for long-wavelength tearing resonant at radii where  $q(r) = m/n$ . Note in figure 5(b) that  $\chi_e$  for PPCD plasmas is greatly reduced in the core, inside the  $q = 0$  toroidal field reversal surface where the density of  $m = 1$  tearing mode resonant surfaces is greatest and the stochasticity most intense in standard plasmas [15]. (For reference,  $q(r)$  has a shape similar to  $E_{\parallel}(r)$  in figure 1(a) for standard plasmas, both of which resemble the toroidal field  $B_{\phi}(r)$  profile.) The broad spectrum of high- $n$ ,  $m = 1$  modes resonant at mid-radius must therefore be strongly influenced by PPCD. The fluctuation reduction shown in figure 2(b) is the total spectral rms, dominated by the largest mode  $m = 1$ ,  $n = 6$  resonant near the magnetic axis ( $q(0) \approx 0.2$ ). The amplitude reduction of the higher- $n$  modes is greater, typically by a factor of 3 to 5.

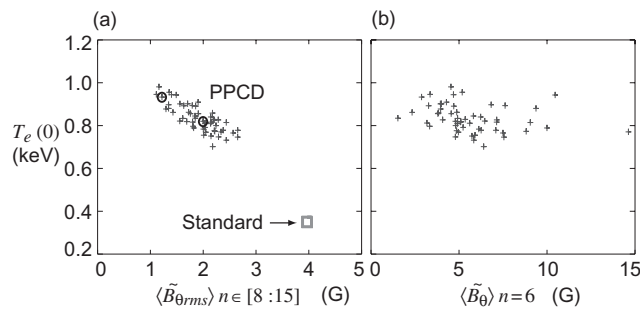


**Figure 9.** (a) Core  $T_e(0)$  at  $t = 18$  ms versus the time-averaged (12–18 ms) rms fluctuation amplitude  $\langle \tilde{B}_{\theta rms} \rangle$  summed for modes  $n \in [8 : 15]$ . (b) Core  $T_e(0)$  versus time-averaged amplitude  $\langle \tilde{B}_{\theta 6} \rangle$  of the dominant mode  $n = 6$  for the same set of plasmas as in (a). These data are for 0.4 MA plasmas with  $n = (0.95 \pm 0.05) \times 10^{19} \text{ m}^{-3}$ . The two circled data points in (a) are referenced in figure 10.

The maximum  $T_e(0)$  achieved during PPCD—a good single indicator of energy confinement in an Ohmically heated plasma—occurs when the time-average amplitudes of the mid-radius modes are smallest. This is shown in figure 9(a), where  $T_e(0)$  near the end of PPCD ( $t = 18$  ms in figure 2) is plotted against the rms fluctuation amplitude  $\tilde{B}_{\theta\text{rms}} = [\frac{1}{2} \sum_n \tilde{B}_{\theta n}^2(a)]^{1/2}$  summed for modes in the range  $n \in [8:15]$  and time-averaged from the start-to-end of PPCD ( $t = 12\text{--}18$  ms in figure 2). The data points labelled ‘+’ are measurements from individual PPCD plasmas with the same current and density formed with identical programming. The data point labelled ‘Standard’ is plotted for the  $T_e(0)$  and high- $n$  rms mode amplitude in standard plasmas with the same current and density. The variation in degree of fluctuation reduction for individual plasmas reveals a clear correlation of higher  $T_e(0)$  with sustained low amplitudes of the mid-radius resonant modes  $n \geq 8$  during PPCD. A double-filter soft-x-ray measurement of  $T_e(0)$  is used for the PPCD plasmas in this analysis to maximize the ensemble size and to provide better temporal resolution than available from Thomson scattering. The ratio of soft-x-ray emission filtered through 725 and 250  $\mu\text{m}$  thick Be foils varies linearly with  $T_e(0) < 1.0$  keV and is accurate for  $T_e(0) \gtrsim 0.5$  keV, limited by small flux through the 725  $\mu\text{m}$  foil. The x-ray ratio is calibrated to Thomson scattering data measured at  $r/a \leq 0.2$  in a subset of the PPCD plasmas.

To better illustrate the impact of variable fluctuation amplitude, figure 10 shows the time evolution of  $T_e(0)$  along with several mode amplitudes for two representative plasmas in figure 9. Three mode amplitudes are shown in figure 10: (b) the dominant  $n = 6, m = 1$  mode resonant nearest the magnetic axis in the core, (c) the rms amplitude,  $\tilde{B}_{\theta\text{rms}}$ , of the mid-radius resonant modes  $n \in [8:15]$ , and (d) the  $n = 1$  mode, which is the largest of the  $m = 0$  modes resonant at the toroidal field reversal surface in the edge. The left-side panels in figure 10 are for the circled ‘+’ data point with one of the highest temperatures  $T_e(0) \approx 0.95$  keV. The right-side panels are for the circled ‘+’ data point with  $T_e(0) \approx 0.8$  keV, the shot-average temperature.

The distinguishing behaviour is that the mid-radius modes, represented by  $\tilde{B}_{\theta\text{rms}}$  in figure 10(c), promptly fall to low amplitude in the ‘hottest’ plasmas, whereas there is a delay in their reduction in the ‘hotter’ plasmas (relative to the start of PPCD). All of the  $n \geq 8$

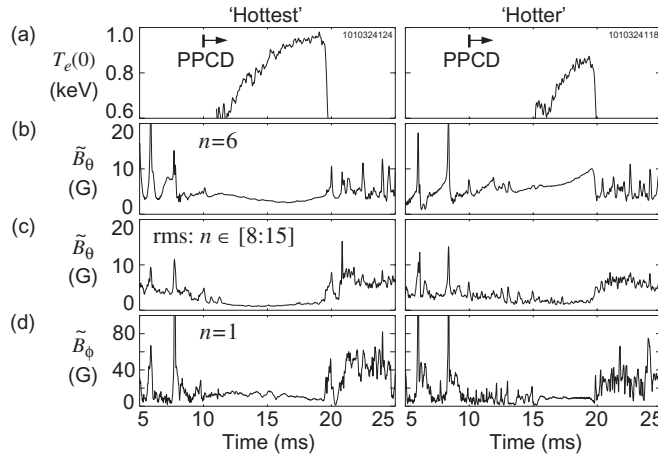


**Figure 10.** (a) Core electron temperature and (b)–(d) representative  $n$ -mode amplitude evolution for two of the PPCD plasmas shown in figure 9. The left-side panels are for the circled data point with one of the highest temperatures, and the right-side panels are for the circled data point in the middle of the distribution. The  $T_e(0)$  evolution is from the Thomson-calibrated soft-x-ray ratio measurement.

modes exhibit similar behaviour, and hence, when this group of modes is smallest, magnetic stochasticity is minimized in the middle region of the plasma (possibly eliminated), and the local  $\nabla_r T_e$  gradient increases, leading to a high core  $T_e(0)$ . The longer the mid-radius modes remain small, the higher  $T_e$  becomes. The  $n = 1$  mode is small in both cases in figure 10(d), an important requirement to achieve high-temperature PPCD plasmas; small mid-radius modes correlate with small  $m = 0$  modes [4].

The  $n = 6$  amplitude is similar for the two cases in figure 10(b), but this mode varies greatly shot-to-shot. Figure 9(b) shows  $T_e(0, t = 18 \text{ ms})$  versus the time-average  $n = 6$  amplitude for the same set of shots as figure 9(a). Two striking features are revealed in the figure 9 data. First, the correlation between  $T_e(0)$  and the dominant—and therefore total—fluctuation amplitude is weak. Second, the temperature in the core is weakly influenced by the nearest resonant mode. Both features are understandable, considering the nature of stochastic magnetic transport. The core temperature is being supported by low heat conductivity in the middle region of the plasma where many high- $n$  modes are resonant. The large  $n = 6$  mode resonant in the core weakly impacts global confinement. This is analogous to the weak impact of  $m = 1, n = 1$  sawtoothing on tokamak plasma confinement when the  $q = 1$  surface remains close to the magnetic axis. Note that some PPCD plasmas in figure 9 have simultaneously one relatively large core-resonant mode and a broad spectrum of small higher- $n$  modes. This combination supports a hope that improved-confinement might occur in a RFP plasma that self-organizes through the ‘single-helicity’ dynamo.

The trend in figure 9(a) for a continual increase in  $T_e(0)$  with a reduction in the magnetic fluctuation amplitude suggests that stochastic transport may still be the dominant energy loss mechanism during PPCD. Note, however, that the 20- to 30-fold reduction of  $\chi_e$  in the core is larger than a typical  $\sim 7$ -fold reduction of  $\langle \tilde{B}_{\text{rms}}^2 \rangle$  for the mid-radius resonant modes; so the  $\chi_e$  reduction is greater than expected from the  $\tilde{B}^2$ -scaling characteristic of stochastic transport. The mid-radius rms fluctuation amplitude is usually not constant in time, as in the right-side panels in figure 10(c), and so the simple time-average amplitude used in figure 9 does not capture the possibility of a dynamic change in the nature of transport during PPCD when the fluctuation falls to its lowest amplitude. Single-shot, spatially resolved local transport analysis is required to examine such changes. A new 20-point Thomson scattering diagnostic, currently being installed on MST, will greatly facilitate single-shot analysis. The  $v_{\parallel}$ -independent diffusion of fast electrons discussed above in section 3 is clearer evidence for a transition to nonstochastic transport, which might have a complicated  $\tilde{B}$ -dependence.

## 5. Summary and discussion

Energy confinement comparable with tokamak quality has been obtained in the MST RFP at a high beta and low toroidal magnetic field. Magnetic fluctuations, which cause magnetic stochasticity in the core of standard RFP plasmas, are reduced by inductive current drive targeted to the edge region of the plasma. A dramatic improvement in confinement results. The electron temperature forms a radial gradient that extends into the core, and the peak temperature reaches  $T_e(0) = 1.3 \text{ keV}$  in 0.5 MA plasmas. The local electron heat diffusivity in the core decreases by a factor  $\sim 30$ -fold to  $\chi_e \sim 5 \text{ m}^2 \text{ s}^{-1}$ . This is comparable with the heat transport observed in tokamak plasmas of the same size and current. The global energy confinement increases 10-fold to 10 ms, to within a factor of 2 of the expected global confinement for a tokamak of the same size and current. Fast electrons  $> 100 \text{ keV}$  are confined, and Fokker–Planck modelling infers that the diffusion of these high-energy electrons is independent of their parallel velocity and therefore not magnetic in nature. Restoration of at least some closed flux surfaces are implied. A strong correlation between high core temperature and low amplitude

$m = 1, n \geq 8$  modes reveals the importance of sustained reduction of resonant tearing in the middle region of the plasma, inside the  $q = 0$  surface where the density of resonant surfaces is highest. These confinement improvements occur with simultaneously high  $\beta_{\text{tot}} \leq 15\%$  and with a magnetic field strength ten times lower than a tokamak of the same size and current.

The inductive PPCD technique used to reduce the tearing and improve confinement is inherently transient. Long-duration sustainment of the current with simultaneous control of tearing instability is clearly challenging, especially considering the lack of a significant pressure-driven bootstrap current in the RFP. Identification of efficient, yet flexible, current drive for the RFP is therefore crucial. Recent analysis of an inductive ‘self-similar’ current ramp-down scenario suggests that optimization of PPCD-like control could lead to a pulsed-current reactor solution [32]. Steady toroidal induction with RF current drive targeted to the outer region of the plasma could also lead to a plausible pulsed-current solution. Two different waves are being investigated at low power in MST, the lower hybrid wave (800 MHz) and the electron Bernstein wave ( $\sim 3.5$  GHz). No substantial RF has ever been injected into an RFP plasma, and so a staged approach to high-power experiments is planned. Theoretical ray tracing and wave damping studies indicate  $\sim 2$  MW of RF power is required for PPCD-equivalent current drive in MST [22, 23].

Steady-state solutions for a current-profile-controlled RFP are yet more challenging. Full RF sustainment (or other noninductive current drive) is unlikely to be feasible, given the relative inefficiency of current drive. Quasi-steady-state solutions are more feasible. For example, oscillating field current drive (OFCD) was proposed in the 1980s as the ideal solution to RFP current sustainment [33]. The inductive toroidal and poloidal loop voltages are oscillated purely sinusoidally, and their product produces DC injection of magnetic helicity to sustain DC current. OFCD is based on self-organization and dynamo physics, and so it is likely to have confinement issues similar to those for steady toroidal induction. However, as an example hybrid solution, an OFCD current ramp-up followed by a self-similar current ramp-down might allow pulsed-burn reactor scenarios in which the current is never fully off, minimizing the cyclical mechanical stress associated with pulsed current. The confinement during the OFCD current ramp-up would only need to be good enough for efficient inductive current drive, with fusion-relevant temperatures maintained during the PPCD-like current ramp-down. Experiments with OFCD at low power have been initiated on MST to test partial current drive and examine the physics issues. A first result is that partial current drive and anti-current drive are observed as the relative phase between the loop voltage oscillations is changed, in agreement with helicity balance expectations. A recent three-dimensional nonlinear resistive MHD computational study has also been completed that firms up the physics basis and illuminates differences in dynamo behaviour relative to steady-induction [34].

The self-organization path forward for the RFP has seen new life recently with the observation of a ‘single-helicity’ dynamo in MHD computation [18, 19]. Instead of having multiple tearing modes, as in the standard RFP, the single-helicity dynamo operates with one relatively large tearing mode. All other tearing modes remain small, which implies the elimination of magnetic stochasticity, or at least greatly reduced stochasticity. The confinement properties of an RFP self-organized with a single mode are likely to be much better as a result. The PPCD result showing that good confinement occurs with small mid-radius resonant modes and simultaneously one large core-resonant mode provides experimental evidence in support of this possibility. However, the one mode observed in MHD computation is substantially larger than seen in any PPCD plasma to date. Spontaneous partial transitions to a single-helicity dynamo, called ‘quasi-single-helicity’ (QSH), are observed in all RFP plasmas [20]. In QSH plasmas, one mode grows larger, while the other modes remain about the same amplitude. An increase in the electron temperature is observed to occur inside the island of the dominant mode, indicative of reduced magnetic stochasticity inside the island, but the global energy

confinement is not significantly altered during QSH, presumably because the nondominant modes are not sufficiently reduced in amplitude.

Plausible pulsed and steady-state current drive scenarios for the single-helicity RFP are conceptually simpler than for the current-profile-controlled RFP. The pulsed case is just toroidal induction, which is well-established and efficient. A steady-state, single-helicity RFP driven by OFCD is especially attractive, but the recent computational study cited above [34] did not find single-helicity dynamo as the default natural solution. An important direction for future research is finding a means to stimulate single-helicity dynamo formation. Self-organization promises simplified current sustainment, but only if the required dynamo does not couple to confinement. The self-organized and current-profile-controlled paths forward to a sustained RFP with fusion-relevant confinement are complementary and increase the chance of realizing toroidal plasmas with a high beta and minimized magnetic field strength.

### Acknowledgments

The authors wish to thank all members of the MST team for their contributions to the work described in this paper. This work was supported by the US Department of Energy.

### References

- [1] Sarff J S *et al* 1997 *Phys. Rev. Lett.* **78** 62
- [2] Bartiromo R *et al* 1999 *Phys. Rev. Lett.* **82** 1462
- [3] Lanier N E *et al* 2000 *Phys. Rev. Lett.* **85** 2120
- [4] Chapman B E *et al* 2001 *Phys. Rev. Lett.* **87** 205001
- [5] Yagi Y *et al* 2003 *Phys. Plasmas* **10** 2925
- [6] O'Connell R *et al* 2003 *Phys. Rev. Lett.* **91** 045002
- [7] Dexter R N *et al* 1991 *Fusion Technol.* **19** 131
- [8] Ortolani S and Schnack D D 1993 *Magnetohydrodynamics of Plasma Relaxation* (Singapore: World Scientific)
- [9] Anderson J K *et al* 2003 Dynamo-free plasma in the reversed field pinch *Phys. Rev. Lett.* submitted
- [10] Anderson J K *et al* 2003 Equilibrium reconstruction in the Madison Symmetric Torus reversed field pinch *Nucl. Fusion* submitted
- [11] Brower D L *et al* 2002 *Phys. Rev. Lett.* **88** 185005
- [12] Craig D *et al* 2001 *Rev. Sci. Instrum.* **72** 1008
- [13] Ji H *et al* 1996 *Phys. Plasmas* **3** 1935
- [14] Den Hartog D J *et al* 1999 *Phys. Plasmas* **6** 1813
- [15] Biewer T M *et al* 2003 *Phys. Rev. Lett.* **91** 045004
- [16] Stoneking M R *et al* 1998 *Phys. Plasmas* **5** 1004
- [17] Cappello S and Biskamp D 1996 *Nucl. Fusion* **36** 571
- [18] Cappello S and Paccagnella R 1992 *Phys. Fluids B* **4** 611
- [19] Finn J *et al* 1992 *Phys. Fluids B* **4** 1262
- [20] Martin P *et al* 2003 *Nucl. Fusion* **43** at press
- [21] Sarff J S *et al* 1994 *Phys. Rev. Lett.* **72** 3670
- [22] Uchimoto E *et al* 1994 *Phys. Plasmas* **1** 3517
- [23] Forest C B *et al* 2000 *Phys. Plasmas* **7** 1352
- [24] Ding W X *et al* 2003 *Phys. Rev. Lett.* **90** 035002
- [25] Chapman B E *et al* 2002 *Phys. Plasmas* **9** 2061
- [26] Rechester A B and Rosenbluth M N 1978 *Phys. Rev. Lett.* **40** 38
- [27] Reardon J *et al* 2001 *Rev. Sci. Instrum.* **72** 1
- [28] Den Hartog D J *et al* 2000 *Plasma Phys. Control. Fusion* **42** L47
- [29] ITER Physics Expert Groups on Confinement and Transport and Confinement Modelling and Database 1999 *Nucl. Fusion* **39** 2175
- [30] O'Connell R *et al* 2003 *Rev. Sci. Instrum.* **74** 2001
- [31] Harvey R A 1992 *GA Report* GA-A20978
- [32] Nebel R A *et al* 2002 *Phys. Plasmas* **9** 4968
- [33] Bevir M K *et al* 1984 *Phys. Fluids* **28** 1826
- [34] Ebrahimi F *et al* 2003 *Phys. Plasmas* **10** 999